

Possible ‘‘Magnéli’’ phases and self-alloying in the superconducting sulfur hydride

Ryosuke Akashi^{1,*}, Wataru Sano^{2,3}, Ryotaro Arita^{3,4}, and Shinji Tsuneyuki^{1,5}

¹*Department of Physics, The University of Tokyo, Hongo, Bunkyo-ku, Tokyo 113-0033, Japan*

²*Department of Applied Physics, The University of Tokyo, Hongo, Bunkyo-ku, Tokyo 113-8656, Japan*

³*RIKEN Center for Emergent Matter Science, Wako, Saitama 351-0198, Japan*

⁴*JST ERATO Isobe Degenerate π -Integration Project,*

Advanced Institute for Materials Research (AIMR),

Tohoku University, Sendai, Miyagi 980-8577, Japan and

⁵*Institute of Solid State Physics, The University of Tokyo, Kashiwa, Chiba 277-8581, Japan*

(Dated: June 11, 2022)

We theoretically give an infinite number of metastable crystal structures for the superconducting sulfur hydride H_xS under pressure. It has been thought that theoretically predicted structures of H_2S and H_3S exhibit low and high T_c in the experiment, respectively. The newly found structures are long-period modulated crystals where slab-like H_2S and H_3S regions intergrow in a microscopic scale. The extremely small formation enthalpy for the H_2S – H_3S boundary indicated with the first-principles calculations suggests possible alloying of these phases through formation of local H_3S regions. The modulated structures and gradual alloying transformations between them could prevail in the experimental samples and could be key ingredients for understanding peculiar pressure dependence of T_c in sulfur hydride observed experimentally.

PACS numbers: 61.50.-f, 81.10.Aj, 61.66.Fn, 74.62.Fj

Sulfur hydride has recently been found to become superconductor at extremely high pressure around 200 K [1, 2]. This is the first achievement of superconducting transition temperature (T_c) exceeding the nitrogen melting point among the conventional phonon mediated superconductors [3], as well as it has broken the long-standing record of 160 K in mercury-cuprate [4–7].

A remarkable feature observed in this superconducting phenomenon is pressure and annealing-scheme dependences of T_c [1, 2]. (i) When the pressure ($>\sim 100$ GPa) is applied to the H_2S sample at room temperatures and afterwards cooled down, the observed T_c s amount to over 150 K, with 203K being the maximum value (open circle in Fig. 1). (ii) By pressurizing at temperature around 100 K, on the other hand, the observed T_c remains low and next rapidly increases (open square in Fig. 1). Although this behavior suggests a variety of structural phases and their peculiar properties, efficient experimental observations have been obstructed by the extremely high pressure. Instead, first-principles calculations have provided insights for the superconducting phases. It is now established that some of the observed values of T_c with the low- and high- T schemes are well reproduced [9–13, 15] with crystal structures predicted for compositions of H_2S , as well as H_3S [9, 10] (See Fig. 1). However, consistent understanding on the observed behavior still remains unprecedented. In particular, no clear explanation on the rapid increase of T_c with the low- T scheme has been given, despite accumulated first-principles proposals of candidate structures with various composition of H_xS [13–16].

The current theoretical attempts have focused on the possible understanding with a minimal number of distinct structural phases. Rather, we provide a different

view: Not only distinct phases but also their mixture have vital roles. Specifically, we find an infinite number of metastable crystal structures having compositions H_xS_{1-x} with $2/3 < x < 3/4$, which have not been reported

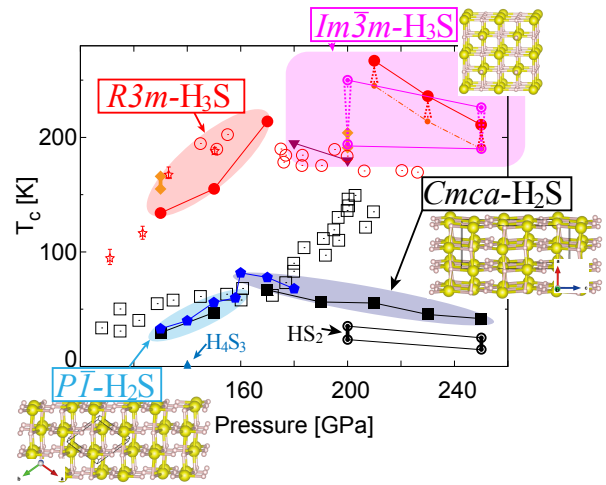


FIG. 1: Experimentally observed T_c (open circle, square [1] and star with error bar [8]) compared with the first-principles calculations (solid symbols). The latter data are taken from Ref. 9 (pentagon), Ref. 10 (rhombus), Ref. 11 (inverted triangle), Ref. 12 (circle and square), Ref. 13 (double circle), Ref. 14 (triangle). The data points in the shaded areas have been obtained from the corresponding predicted crystal structures [9, 10], respectively. Note that $R3m$ - H_3S is a trigonally distorted variant of $Im\bar{3}m$ - H_3S . The upward (downward) wedges indicate the enhancement (suppression) of T_c due to the plasmon effect [12] (phonon anharmonicity [13]), whereas the vertical bars connecting some points indicate the T_c variation with the empirical Coulomb parameter μ^* [10, 13].

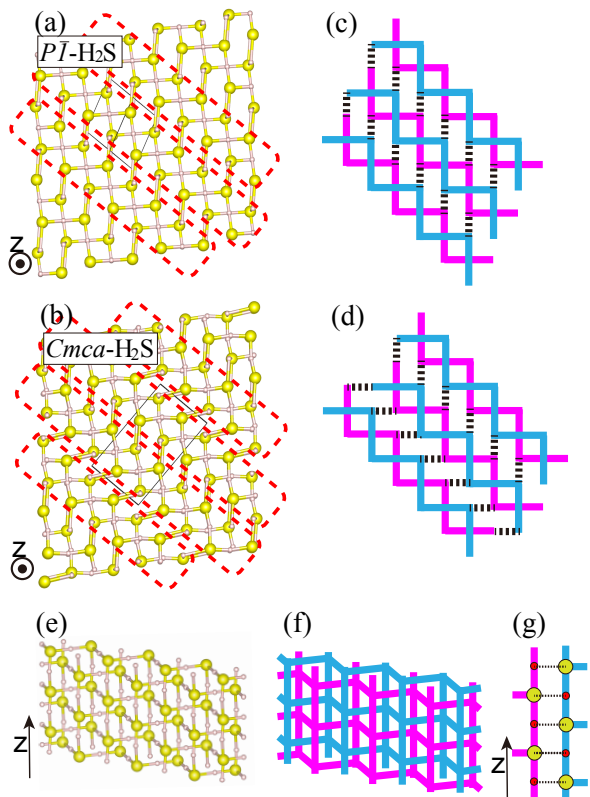


FIG. 2: (a) (1 1 0) view of $P\bar{1}$ -H₂S and (b) (1 0 0) view of $Cmca$ -H₂S, where the unit cells are depicted in thin lines. The common units are indicated by red lines. (c)–(d) Schematic pictures of (a) and (b), respectively, where the bond depicted by panel (g) is indicated by thick dashed lines. (e)–(f) The fundamental unit structure, “interlaced square nets” and its schematic picture. In panel (f), sulfur and hydrogen atoms are located at the corners and the centers of the edges, respectively. (g) Bonding structure in panels (c) and (d), where sulfur and hydrogen atoms are depicted in yellow and red, respectively.

in the first-principles structure-search studies. They can be understood as long-period modulated crystals formed by stacking the H₂S and H₃S slab-like structures, which are reminiscent of the Magnéli phases in transition-metal oxides [17]. All these structures are thermodynamically as stable as the complete separation to H₂S and H₃S phases. This suggests that the microscopic *intergrowth* of the H₂S and H₃S regions requires little activation enthalpy and therefore occurs ubiquitously in the experimental situation, forming, as it were, slab-alloy phase. We also show that the presence of such alloy phase gives a plausible explanation for the T_c -pressure curve observed experimentally.

We begin with a discussion of the hidden similarity between theoretically predicted relevant structures for H₂S and H₃S. $P\bar{1}$ -H₂S and $Cmca$ -H₂S (Fig. 1) are known to give low T_c values [9, 12], which agree relatively well with the experimental values with the low- T annealing for the

low-pressure regime. $Im\bar{3}m$ -H₃S (Fig. 1) gives theoretical T_c consistent with the high- T annealing cases, and its presence is recently confirmed with the X-ray diffraction measurements [8, 14, 18]. Seen from the (1 1 0) direction [(1 0 0) direction] in the setup of Ref. 9, one can notice that $P\bar{1}$ - and $Cmca$ -H₂S can be decomposed into the common unit structures [Figs. 2(a)–(d)]: Two H₂S square nets interlaced with each other [Fig. 2(e)–(f)]. The units of this shape are bound with each other so that sulfur atoms adopt local FCC-like stacking [Fig. 2(g)] [19]. The $P\bar{1}$ and $Cmca$ structures can now be distinguished by the configuration of the inter-unit bonding. The uniform (alternating) bonding orientation yields the $P\bar{1}$ ($Cmca$) structure. An important thing is that the $Im\bar{3}m$ -H₃S structure can also be formed with the present unit by binding them so that the vertical edges are shared [Fig. 3(c)].

The unit-based perspective for H₂S and H₃S is indeed helpful for us to construct a group of metastable structures. In a wide variety of materials such as metal oxides, multiple crystalline phases with slightly different stoichiometries emerge depending on the bonding between the unit complexes [20, 21]. One of such examples is the Magnéli phases in molybdenum- [17, 22, 23], tungsten- [17, 24], titanium- [25–28], and vanadium-oxides [29–32], where two-dimensional defects (or *crystallographic shear* [33]) of edge- or face-sharing bonding between metal-oxide complexes are periodically formed. On the analogy to them, here we consider possible crystalline phases formed by the structural H₂S unit.

We first define the three types of the inter-unit bonding (Fig 3 (a)–(c)): bonding α and $\bar{\alpha}$ correspond to the

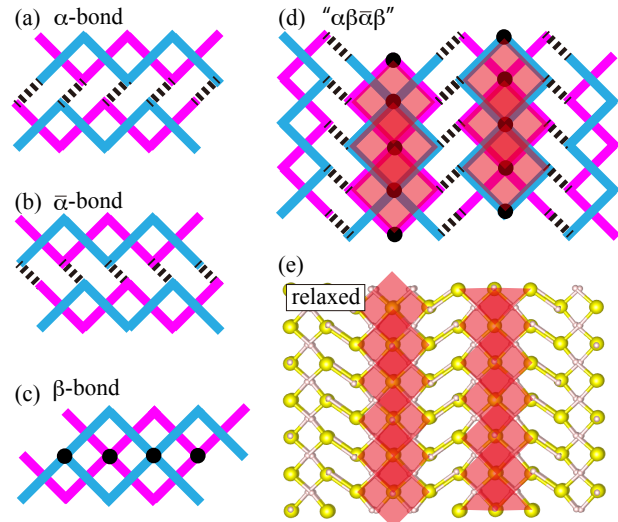


FIG. 3: (a)–(c) Definitions of the inter-unit bonding. (d) Long-period modulated structure generated from permutation “ $\alpha\beta\bar{\alpha}\beta$ ” and (e) its relaxed counterpart (see the main text). The $Im\bar{3}m$ -H₃S regions are shaded in red.

two bonding orientations seen in $Cmca$ - H_2S , respectively, whereas bonding β corresponds to the bond sharing the edge. With this definition, by arranging the units side by side and next assigning any type of bonding for every neighboring pair of units, we can generate a crystal structure formed by the units. In this sense, every circular permutation composed of desired numbers of α , $\bar{\alpha}$ and β yields a corresponding long-period modulated crystal structure. Any structures generated in this way have intermediate composition H_xS_{1-x} ($2/3 \leq x \leq 3/4$), whose unit cells are composed of $H_{4N-k}S_{2N-k}$ with N and k being the period of the permutation and the number of β , respectively. The “ $\alpha\beta\bar{\alpha}\beta$ ” structure is exemplified in Fig. 3(d), whose unit-cell formula is $H_{14}S_6$. As the number of β increases, H_3S -like structural regions grow [Fig. 3 (d)(e)]. Note that $P\bar{1}$ - H_2S , $Cmca$ - H_2S , and $Im\bar{3}m$ - H_3S are generated by permutations “ α ” (also “ $\bar{\alpha}$ ”; see Supplemental Materials [34]), “ $\alpha\bar{\alpha}$ ”, and “ β ”, respectively.

Using the structures thus generated from the permutations of period 2, 3, and 4 as inputs, we carried out the first-principles structure optimization for various pressures. Our calculations were done using the first-principles code package QUANTUM ESPRESSO [35] with the generalized-gradient approximation for the exchange-correlation potential [36]. The unit-cell compositions of the resulting structures are H_7S_3 , $H_{10}S_4$, $H_{11}S_5$, $H_{12}S_6$, $H_{13}S_5$, $H_{14}S_6$, $H_{15}S_7$, and $H_{16}S_8$, respectively. Detailed conditions of the calculations are summarized in Supplemental Materials [34]. We have found that the formation enthalpy $\Delta H(H_xS_{1-x})$ for all the resulting structures satisfy $\Delta H(H_2S) \gtrsim \Delta H(H_xS_{1-x}) \gtrsim \Delta H(H_3S)$ (Fig. 4). We have also confirmed that all these structures retain the bonding characteristics in their initial structures [Fig. 3(e)]. Namely, every different permutation gives different optimum metastable structures where well-defined bcc- H_3S slab regions emerge. To our knowledge, the structures of this group have not been reported in the previous structure-search studies [9–11, 13–16], which is probably due to their large and anisotropic unit cells. Although we do not examine the $N \geq 5$ cases here, an infinite number of metastable structures are expected to be obtained in this way.

Remarkably, the values of formation enthalpy relative to the complete decomposition into H_2S and H_3S are wholly within 50 K per atom [insets of Fig. 4(a)–(d)]. This dependence is not an indication of trivial phase separation into H_2S and H_3S because the two regions *intergrow* in a microscopic scale in the respective structures (see Fig. 3 (e)). A more appropriate interpretation is that the formation enthalpy for the H_2S – H_3S boundary is extremely small in these structures.

Since H_2S and H_3S are metallic in their pristine forms, we can expect that the intermediate crystal structures are also metallic. To confirm this, we calculated electronic density of states [34] in some optimum structures for H_xS_{1-x} with $x = 2/3$, $7/10$, $10/14$, $13/18$, $25/34$,

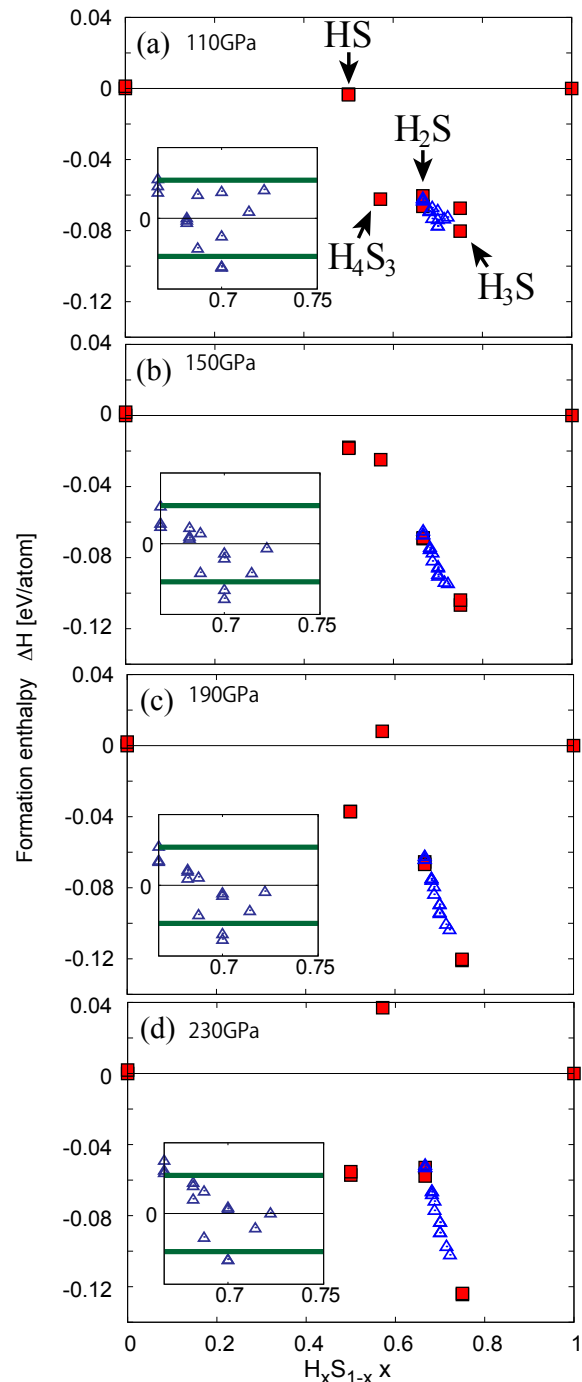


FIG. 4: (a)–(d) Formation enthalpy from the first principles at various pressures. The structures corresponding to the points are summarized in Supplemental Materials [34]. The inset panels focus the region between $x = 2/3$ (H_2S) and $x = 3/4$ (H_3S), where the formation enthalpies are measured with respect to the values for the phase separation of H_2S and H_3S . Bold lines indicate ± 50 kelvin.

49/66 and $3/4$ at 170 GPa (Fig. 5, left), which have been generated from the permutations “ α ”, “ $\alpha\beta$ ”, “ $\alpha\beta\beta$ ”, “ $\alpha\beta\beta\beta$ ”, “ $\alpha\beta\beta\beta\beta\beta$ ”, “ $\alpha(\beta \times 15)$ ” and “ β ”, respectively. Clearly, all the spectra show nonzero values at

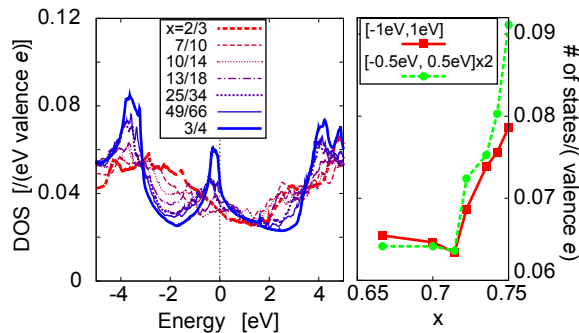


FIG. 5: (left) Density of states (DOS) per valence electron for various compositions. (right) Total number of states per valence electron calculated within the range of $[-1\text{eV}, 1\text{eV}]$ and $[0.5\text{eV}, 0.5\text{eV}]$.

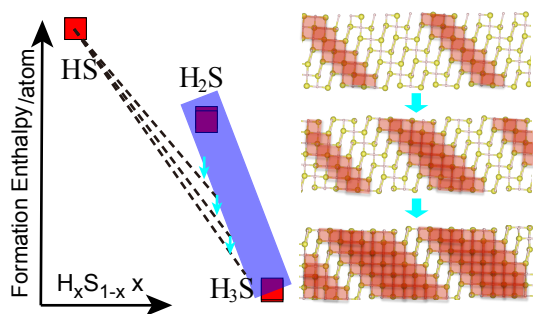


FIG. 6: Schematic picture of a possible transformation path “ α ($\bar{\alpha}$) \rightarrow β +HS”. The shaded area in the left plot represents the multiple intermediate structures, whereas that in the right indicate the H_3S regions.

the Fermi level, indicating the consistent metallicity of the systems. We also observed a peak in the DOS near the Fermi level growing gradually with the increase of x , which evolves into the van-Hove peak found in the pristine $Im\bar{3}m$ - H_3S [10, 15, 37]. More quantitatively, we also calculated the total number of states per valence electron within the range of ± 1 eV ($\approx 5 \times \omega_D$) and ± 0.5 eV ($\approx 2.5 \times \omega_D$) with ω_D being the Debye frequency [10], respectively (Fig. 5, right). These results indicate that the electronic structure is not linearly but at least continuously dependent on the H ratio x . Consequently, we can also expect continuous change of T_c , though more detailed analysis about this point is left for future studies.

Finally, we argue the relevance of the newly found intermediate phases in the experimental situation. We here have to bear in mind that the intermediate structures are *within* the convex hull of the formation enthalpy in the present pressure regime, apart from the narrow range around 110 GPa (Fig. 4 and Ref. [14]). This means that in the compressed H_2S system, these phases do not grow as the decomposition residues of the emergence of H_3S phase, if annealed with enough time and heat. However, the decomposition paths otherwise depend on

the enthalpy barrier from the pristine H_2S structures. The transition between two metastable structures with slightly different x occurs through transformations of a small fraction of α ($\bar{\alpha}$)-type inter-unit bonds to β . This sporadic character of the bonding transformation and the small formation enthalpy for the H_2S - H_3S boundary revealed above suggest that such transition requires little activation enthalpy. The intermediate crystalline phases should thus be observable if H_xS systems exhibit either of the $P\bar{1}$ - or $Cmca$ - H_2S region and next further compressed at low temperature.

We can also find a piece of supporting evidence for this scenario. The H-S ratio of the residual atoms for the α ($\bar{\alpha}$)-to- β bonding transformation is 1:1. On the other hand, the calculated formation enthalpy for HS relative to that for H_2S decreases with compression [see Fig. 4 (a)–(d)]. This pressure-induced phenomenon would encourage the transformation α ($\bar{\alpha}$) \rightarrow β +HS (Fig. 6), which is consistent with the experimentally observed increase of T_c with the low- T scheme (Fig. 1). We hence propose that this behavior is due to the intermediate phases.

We additionally assert that not only the crystalline phase of a single stoichiometry but also nanoscale slab-like regions of the different phases emerge in an ordered and random fashion, similarly to the cases of the microsyntactic intergrowth [30] observed in silicon carbide [38] and metallic oxides including the Magnéli materials [30, 39–42]. The coexistence of them will appear in reality an alloy-like phase formed by the slabs of the metallic H_2S and H_3S . This alloy phase is a compound analog of the classic superconducting alloys formed by elemental metals [43], but quite different from them. The ingredients of the former alloy— H_2S and H_3S slabs—can develop in the common H_2S crystalline phases and therefore, even in the pristine sample, their alloying occurs in the self-contained manner through the structural and stoichiometric transformations.

In summary, we have provided an interpretation based on the common structural unit for the known crystal structures of the low- and high- T_c H_2S and H_3S and thereby found metastable modulated alloy-like structures formed by their microsyntactic intergrowth. The experimentally observed pressure dependence of T_c is reasonably explained with pressure-induced gradual transformations through such alloy phases. The present finding gives a new insight into the high- T_c superconducting phenomena in sulfur hydride that the microscopic mixture of the phases can be ubiquitous.

Acknowledgment. This work was supported by MEXT Element Strategy Initiative to Form Core Research Center in Japan and JSPS KAKENHI Grant Numbers 15K20940 (R. Ak) and 15H03696 (R. Ar) from Japan Society for the Promotion of Science (JSPS). We thank Yinwei Li for sharing structure data for H_4S_3 in arXiv:1508.03900. We also thank Mikhail Eremets, Yoshihiro Iwasa and Hui-hai Zhao for enlightening com-

ments.

SUPPLEMENTAL MATERIALS

Equivalence between the bonding permutations

Here we summarize which permutations yield equivalent and nonequivalent metastable structures. (i) the cyclic variants of any permutations give equivalent structures because of the periodicity of the crystal. (ii) Pairs of permutations exchanged by $\alpha \leftrightarrow \bar{\alpha}$ (e.g., “ $\alpha\bar{\alpha}\beta$ ” and “ $\bar{\alpha}\alpha\beta$ ”) yield pairs of structures exchanged by the mirror plane m_1 (plane perpendicular to the units, see Fig. 7). (iii) Pairs of permutations exchanged by inversion (e.g., “ $\alpha\bar{\alpha}\beta$ ” and “ $\beta\bar{\alpha}\alpha$ ”) yields structures interchanged by global inversion (i). All the permutations related by these three operations yield equivalent structures in that they give equal values of formation enthalpy. Note that the mirror reflection with respect to plane m_2 (plane parallel to the units, see Fig. 7) is represented by the combination of the former operations.

Relaxed structures

We carried out the first-principles structure optimization for the structures summarized in Table I, which resulted in the values of the formation enthalpy depicted in Fig. 4 (triangle). Note that this list exhausts all the possible structures for $N \leq 4$, in that any unlisted permutations can be related to either of the listed ones with the operations summarized in Fig. 7.

The first-principles structure optimization has also been done for other compounds for reference. The squares in Fig. 4 correspond to the body-centered monoclinic (without spatial modulation) and β -Po sulfur

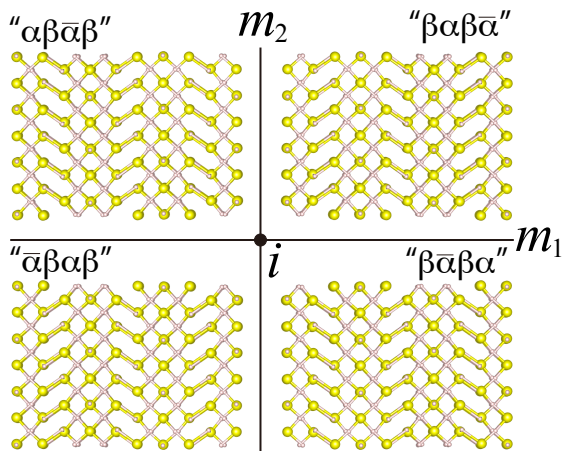


FIG. 7: Relations between the operations on the permutation and structure, exemplified with permutation “ $\alpha\beta\bar{\alpha}\beta$ ”.

(Ref. 44), $I4_1/amd$ - and $C2/m$ -HS (Ref. 13), $Pnma$ - H_4S_3 (Ref. 14), $P\bar{1}$ - and $Cmca$ - H_2S (Ref. 9), $R3m$ - and $Im\bar{3}m$ - H_3S (Ref. 10), and $C2/c$ -H (Ref. 45).

Computational details

The first-principles structure optimizations were carried out using plane-wave pseudopotential calculation codes QUANTUM ESPRESSO [35]. The calculations were done with the generalized-gradient approximation using the exchange-correlation potential with the Perdew-Burke-Ernzerhof parametrization [36]. We used the pseudopotentials for S and H atoms implemented with the Troullier-Martin scheme [46]. The plane-wave energy cutoff was set to 80 Ry. For the structures corresponding to the permutations of $N = 2$, $N = 3$, and $N = 4$ (see Table I), we described the charge density using the \mathbf{k} points on the $4 \times 10 \times 10$, $3 \times 10 \times 10$, and $2 \times 10 \times 10$ meshes (see the next paragraph for the setup of the lattices), respectively, with the first-order Hermite-Gaussian function of width of 0.03 Ry [47]. The electronic densities of states for $P\bar{1}$ - H_2S and $R3m$ - H_3S were calculated with the tetrahedron method [48] using the $33 \times 33 \times 23$ and $33 \times 33 \times 33$ \mathbf{k} -point meshes in the standard lattice setup [9, 10], respectively, whereas those for the intermediate structures corresponding to $N = 2, 3, 4, 8, 16$ were based on the $8 \times 40 \times 40$, $6 \times 40 \times 40$, $4 \times 28 \times 28$ meshes, respectively.

We generated the input unit cells based on the following algorithm. (i) Define the S-H bonding length a , (ii) assuming the first element of the permutation to be α , give the positions for two sulfur and four hydrogen atoms in the Cartesian coordinates by $S_{(1)}=(0, 0, 0)$, $S_{(2)}=(2, 0, 0)$, $H_{(1)}=(0, 0, 1)$, $H_{(2)}=(1, 0, 1)$, $H_{(3)}=(2, 0, 1)$, $H_{(4)}=(1, 0, 0)$ in unit of a . Here and hereafter, $A_{(n)}$ denotes the position of the n th atom of kind A . (iii) if the next element of the permutation is α , generate two sulfur and four hydrogen atoms by $S_{(n)}=S_{(n-2)}+(3, 0, 0)$ and $H_{(n)}=H_{(n-4)}+(3, 0, 0)$; if $\bar{\alpha}$, generate two sulfur and four hydrogen atoms by $S_{(n)}=S_{(n-2)}+(3, 0, 1 \times (-1)^i)$ and $H_{(n)}=H_{(n-4)}+(3, 0, 1 \times (-1)^i)$ for the i th $\bar{\alpha}$; if β , on

TABLE I: The calculated structures in terms of the corresponding permutation and the composition of the unit cell.

N	Permutation	Composition (/unit cell)
2	$\alpha\beta$	H_7S_3
3	$\alpha\alpha\bar{\alpha}$	$H_{12}S_6$
3	$\alpha\alpha\beta, \alpha\bar{\alpha}\beta$	$H_{11}S_5$
3	$\alpha\beta\beta$	$H_{10}S_4$
4	$\alpha\alpha\alpha\bar{\alpha}, \alpha\alpha\bar{\alpha}$	$H_{16}S_8$
4	$\alpha\alpha\alpha\beta, \alpha\alpha\bar{\alpha}\beta, \alpha\bar{\alpha}\alpha\beta$	$H_{15}S_7$
4	$\alpha\alpha\beta\beta, \alpha\bar{\alpha}\beta\beta, \alpha\beta\bar{\alpha}\beta$	$H_{14}S_6$
4	$\alpha\beta\beta\beta$	$H_{13}S_5$

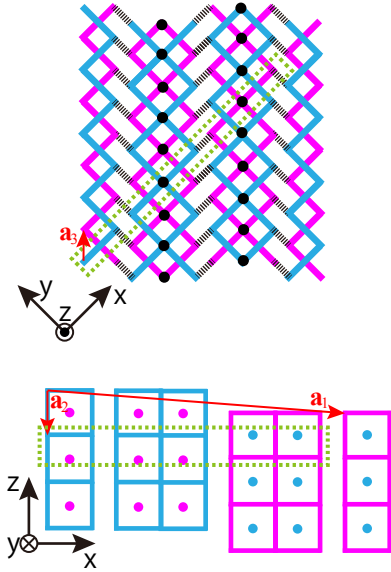


FIG. 8: A scheme of implementing the initial structures, exemplified by the structure “ $\alpha\beta\bar{\alpha}\beta$ ”. The rectangular area drawn with dashed line represents the unit cell, whereas the solid arrows represent the primitive lattice vectors defined in the present scheme. Note that the corners (centers of the edges) of the solid graph are occupied by sulfur (hydrogen) atoms.

the other hand, generate one sulfur and three hydrogen atoms by $S_{(n)}=S_{(n-1)}+(2, 0, 0)$ and $H_{(n)}=H_{(n-3)}+(2, 0, 0)$. (iv) Repeat (ii)–(iii) to the end of the permutation, which yields the unit cell indicated by the dashed line in Fig. 8. (v) Finally define the three lattice vectors as $\mathbf{a}_1 = (3N - k, 0, -l \bmod 2)$, $\mathbf{a}_2 = (0, 0, -2)$, and $\mathbf{a}_3 = (1, 1, 1)$ (see Fig. 8) for the permutation of period $N(\geq 2)$ including l $\bar{\alpha}$ s and k β s. We set $a = 2.8$ Bohr for all the initial structures. We assumed no symmetry during the structure optimization, nor have we specified the symmetries of the final structures. Note that one can also develop different lattice-generation schemes yielding the same structures.

-
- * akashi@cms.phys.s.u-tokyo.ac.jp
- [1] A. P. Drozdov, M. I. Erements, and I. A. Troyan, V. Ksenofontov, and S. I. Shylin, *Nature (London)* **525**, 73 (2015).
- [2] A. P. Drozdov, M. I. Erements, and I. A. Troyan, arXiv:1412.0460.
- [3] J. Bardeen, L. N. Cooper, and J. R. Schrieffer, *Phys. Rev.* **108**, 1175 (1957).
- [4] C. W. Chu, L. Gao, F. Chen, Z. J. Huang, R. L. Meng, and Y. Y. Xue, *Nature (London)* **365**, 323 (1993).
- [5] L. Gao, Y. Y. Xue, F. Chen, Q. Xiong, R. L. Meng, D. Ramirez, C. W. Chu, J. H. Eggert, and H. K. Mao, *Phys. Rev. B* **50**, 4260(R) (1994).
- [6] M. Monteverde, C. Acha, M. Núñez-Regueiro, D. A. Pavlov, K. A. Lokshin, S. N. Putilin, and E. V. Antipov, *EPL (Europhys. Lett.)* **72**, 458(2005).
- [7] N. Takeshita, A. Yamamoto, A. Iyo, and H. Eisaki, *J. Phys. Soc. Jpn.* **82**, 023711 (2013).
- [8] M. Einaga, M. Sakata, T. Ishikawa, K. Shimizu, M. I. Erements, A. P. Drozdov, I. A. Troyan, N. Hirao, and Y. Ohishi, arXiv:1509.03156.
- [9] Y. Li, J. Hao, H. Liu, Y. Li, and Y. Ma, *J. Chem. Phys.* **140**, 174712 (2014).
- [10] D. Duan, Y. Liu, F. Tian, D. Li, X. Huang, Z. Zhao, H. Yu, B. Liu, W. Tian, and T. Cui, *Sci. Reports* **4**, 6968 (2014).
- [11] J. A. Flores-Livas, A. Sanna, and E. K. U. Gross, arXiv:1501.06336.
- [12] R. Akashi, M. Kawamura, S. Tsuneyuki, Y. Nomura, and R. Arita, *Phys. Rev. B* **91**, 224513 (2015).
- [13] I. Errea, M. Calandra, C. J. Pickard, J. Nelson, R. J. Needs, Y. Li, H. Liu, Y. Zhang, Y. Ma, F. Mauri, *Phys. Rev. Lett.* **114**, 157004 (2015).
- [14] Y. Li, L. Wang, H. Liu, Y. Zhang, J. Hao, C. J. Pickard, J. R. Nelson, R. J. Needs, W. Li, Y. Huang, I. Errea, M. Calandra, F. Mauri, and Y. Ma, arXiv:1508.03900.
- [15] N. Bernstein, C. S. Hellberg, M. D. Johannes, I. I. Mazin, and M. J. Mehl, *Phys. Rev. B* **91**, 060511(R) (2015).
- [16] D. Duan, X. Huang, F. Tian, D. Li, H. Yu, Y. Liu, Y. Ma, B. Liu, and T. Cui, *Phys. Rev. B* **91**, 180502(R) (2015).
- [17] A. Magnéli, *Acta Cryst.* **6**, 495 (1953).
- [18] Note that the theoretically predicted $R3m$ distortion is so small as to be difficult to measure in the experiment.
- [19] We can also regard that the dominant inter-unit bonding is the S-S one [9] instead S-H, though this difference does not change the conclusion of the later discussions.
- [20] L. Bragg and G. F. Claringbull, *Crystal Structure of Minerals* (G. Bell and Sons, Ltd., London, 1965).
- [21] L. R. Eyring and L. T. Tai, in *Treatise on Solid State Chemistry: Volume 3 Crystalline and Noncrystalline Solids*, edited by N. B. Hannay (Plenum Press, New York, 1976), Chapter 3.
- [22] L. A. Bursill, *Proc. Roy. Soc. Ser. A* **311**, 1505 (1969).
- [23] D. Wang, D. Su, and R. Schlögl, *Cryst. Res. Technol.* **38**, 153 (2003).
- [24] M. Sundberg and R. J. D. Tilley, *Phys. Stat. Sol. A* **22**, 677 (1974); R. Pickering and R. J. D. Tilley, *J. Solid State Chem.* **16**, 247 (1976).
- [25] S. Andersson, B. Collén, U. Kuylenstierna, and A. Magnéli, *Acta Chem. Scand.* **11**, 1641 (1957); S. Andersson, B. Collén, G. Kruuse, U. Kuylenstierna, A. Magnéli, H. Pestmalis, and S. Åsbrink, *Acta Chem. Scand.* **11**, 1653 (1957).
- [26] O. Terasaki and D. Watanabe, *Jpn. J. Appl. Phys.* **10**, 292 (1971).
- [27] L. A. Bursill and B. G. Hyde, *Prog. Solid State Chem.* **7**, 177 (197).
- [28] S. Harada, K. Tanaka, and H. Inui, *J. Appl. Phys.* **108**, 083703 (2010).
- [29] S. Andersson and L. Jahnberg, *Ark. Kemi* **21**, 413 (1963).
- [30] Y. Hirotsu, Y. Tsunashima, S. Nagakura, H. Kuwamoto, and H. Sato, *J. Solid State Chem.* **43**, 33 (1982).
- [31] P. C. Canfield, J. D. Thompson, and G. Gruner, *Phys. Rev. B* **41**, 4850(R) (1990).
- [32] U. Schwingenschlögl and V. Eyert, *Ann. Phys. (Berlin)* **13**, 475 (2004).
- [33] A. D. Wadsley, in *Fasciculus Extraordinarius Alfred Werner, 1866-1919: Alfred Werner Commemoration Volume* (Verlag Helvetica Chimica Acta, Basel, 1967).
- [34] The equivalence between the permutation, initial crystal structures for the optimization calculations, and computational details are summarized in Supplemental Materials.
- [35] P. Giannozzi *et al.*, *J. Phys.: Condens. Matter* **21**, 395502 (2009); <http://www.quantum-espresso.org/>.
- [36] J. P. Perdew, K. Burke, and M. Ernzerhof, *Phys. Rev. Lett.* **77**, 3865 (1996).
- [37] D. A. Papaconstantopoulos, B. M. Klein, M. J. Mehl, and W. E. Pickett, *Phys. Rev. B* **91**, 184511 (2015).
- [38] H. Sato and S. Shiozaki, *Mat. Res. Bull.*, **9**, 679 (1974).
- [39] D. J. M. Bevan, B. Hudson, and P. T. Moseley, *Mat. Res. Bull.*, **9**, 1073 (1974).
- [40] Y. Hirotsu and H. Sato, *J. Solid State Chem.* **26**, 1 (1978).
- [41] Y. Hirotsu, S. P. Faile, and H. Sato, *Mat. Res. Bull.*, **13**, 895 (1978).
- [42] Y. Hirotsu and H. Sato, *Mat. Res. Bull.*, **15**, 41 (1980).
- [43] B. T. Matthias, T. H. Geballe, and V. B. Compton, *Rev. Mod. Phys.* **35**, 1 (1963).
- [44] O. Degtyareva, E. Gregoryanz, M. Somayazulu, H. K. Mao, and R. J. Hemley, *Phys. Rev. B* **71**, 214104 (2005).
- [45] C. J. Pickard and R. J. Needs, *Nat. Phys.* **3**, 473(2007).
- [46] N. Troullier and J. L. Martin, *Phys. Rev. B* **43**, 1993 (1991); <http://www.abinit.org/downloads/psp-links/psp-links/gga.fhi>.
- [47] M. Methfessel and A. T. Paxton, *Phys. Rev. B* **40**, 3616 (1989).
- [48] P. E. Blöchl, O. Jepsen, and O. K. Andersen, *Phys. Rev. B* **49**, 16223 (1994).